2011 American Control Conference
on O'Farrell Street, San Francisco, CA, USA
June 29 - July 01, 2011

Observability Analysis of an Inertial Navigation System with Stationary Updates

Arvind Ramanandan Anning Chen Jay A. Farrell

Abstract— **Stationary measurement updates offer the possibility of containing errors in velocity, biases and attitude even during periods of GPS unavailability, given the information that the rover is not moving. Automated detection of appropriate instances of stationarity is possible, given a recently proposed frequency domain method based on IMU data.**

In this paper we focus on analytical and numerical evaluation of observability of error states of an INS aided with stationary updates. The null space of the continuous time observability gramian is evaluated for various motion scenarios typically occurring in a land vehicle.

I. Introduction

IMU based dead-reckoning is a well known localization approach. Inertial sensor measurements are affected by non-zero, slowly changing errors herein referred to as sensor biases. Due to the presence of these biases, localization errors in a dead-reckoning INS can grow to the meter level in tens of seconds. Sensor biases are nuisance parameters and should be estimated to improve localization performance. Hence, aiding measurements like GPS, are usually integrated with an inertial system to estimate these bias as a portion of the error state vector. But in situations like an urban canyon, where the line of sight to satellites is intermittent, GPS measurements are not available reliably, or are affected by large multipath errors causing INS errors to diverge quickly, motivating the need for an alternative type of updates. Several authors have suggested stationary updates as one such alternative aiding technique [2], [4], [7], [12], [13], [14], [17] etc.

Stationary updates are pseudo-measurements that constrain the velocity and angular rotation rate of the rover with respect to earth to zero. If it is given that the rover is stationary, then stationary updates correct errors in velocity and gyroscope biases. In [15], the authors proposed a frequency domain approach using IMU data to detect the stationarity condition. The focus in this paper is on theoretical evaluation of observability in an inertial navigation system aided by stationary updates.

Observability of INS error states using GPS under various maneuvering scenarios is well understood [1], [3], [8], [9], [16], but such an analysis is absent in the literature for an INS aided by stationary updates. This paper derives the observability conditions for a stationary-aided INS, under situations where the rover is in motion and stationary during different time intervals. There are three main motion scenarios that occur frequently on land vehicles. They are: (i) Stationary rover, (ii) Rover decelerating to a stop (ii) Rover starting and ending in stationarity. In subsequent sections, these motion scenarios are rigorously defined and the observability gramian is analyzed.

The structure of the paper is as follows: Section II deals with the background by providing notation and sensor modeling. It also derives the continuous time state transition matrix for an error state INS. Section III defines various motion scenarios and analyzes the observability gramian. It also derives a basis for the unobservable subspace wherever applicable. Section IV discusses the observability results from a state estimation view point and provides simulation results supporting the theoretical conclusions of Section III. Section V concludes the paper.

A. Notation

Let the symbols b, n, e and i in either the superscript or subscript denote the body, navigation, Earth Centered Earth Fixed (ECEF) and inertial frames respectively. The navigation frame is a tangent plane with known position and orientation relative to the ECEF frame. The symbol ${}^{a}\boldsymbol{x}$ expresses the vector $\boldsymbol{x}$ in the a frame. The symbol ${}^{c}\boldsymbol{\omega}_{ab}$ denotes the angular rate of rotation of frame b relative to frame a as represented in the c frame. Let a and b frames be such that their origins coincide and their relative orientations be known. If ${}^{a}\boldsymbol{v}$ denotes a free vector $\boldsymbol{v}$ in the a frame, then the rotation matrix ${}^{b}_{a}\boldsymbol{R}$ is used to transform it to the b frame as ${}^{b}\boldsymbol{v} = {}^{b}_{a}\boldsymbol{R}\,{}^{a}\boldsymbol{v}$. For any vector $\boldsymbol{v}$, the symbol $[\boldsymbol{v}\times]$ denotes the matrix cross product form for $\boldsymbol{v}$ such that $\boldsymbol{v}\times\boldsymbol{u} = [\boldsymbol{v}\times]\boldsymbol{u}$. The symbols $\hat{\boldsymbol{x}}$, $\tilde{\boldsymbol{x}}$ denote an estimate and measurement of $\boldsymbol{x}$ respectively. The estimation error $\delta\boldsymbol{x}$ is defined as $\delta\boldsymbol{x} = \boldsymbol{x} - \hat{\boldsymbol{x}}$. The symbol ${}^{c}\dot{\boldsymbol{x}}$ denotes the time derivative of ${}^{c}\boldsymbol{x}$ in the c frame.

II. Background

Let the navigation state of the rover be defined as $\bar{\mathbf{x}}^{\top} = \begin{bmatrix} {}^{n}\boldsymbol{p}_{nb}^{\top} & {}^{n}\boldsymbol{v}_{nb}^{\top} & \boldsymbol{\Theta}^{\top} \end{bmatrix}$, where ${}^{n}\boldsymbol{p}_{nb} \in \mathbb{R}^3$ $\left({}^{n}\boldsymbol{v}_{nb} \in \mathbb{R}^3\right)$ denotes the position (velocity) of the body frame in the navigation frame and the Euler angles $\boldsymbol{\Theta}$ denote the attitude of the body frame relative to the navigation frame.

A. Sensor modeling

The IMU is equipped with six inertial sensors: 3 accelerometers and 3 gyroscopes. The sensitive axis of the sensors are aligned along the standard basis of the b frame.

A. Ramanandan is a Ph.D. Candidate at Department of Electrical Engineering, University of California, Riverside, CA, 92521. aramanandan@ee.ucr.edu

A. Chen is a Ph.D. Candidate at Department of Electrical Engineering, University of California, Riverside, CA, 92521. achen@ee.ucr.edu

J. A. Farrell is with the Faculty of Department of Electrical Engineering, University of California, Riverside, CA, 92521. farrell@ee.ucr.edu

The strapdown inertial sensor measurements in the body frame are modeled in continuous time as

$$ {}^{b}\tilde{\boldsymbol{y}} = {}^{b}\boldsymbol{y} + {}^{b}\boldsymbol{b} + \boldsymbol{n} $$

where ${}^{b}\boldsymbol{y}^{\top} = \begin{bmatrix} {}^{b}\boldsymbol{f}^{\top} & {}^{b}\boldsymbol{\omega}_{ib}{}^{\top} \end{bmatrix}$ and

$$ {}^{b}\boldsymbol{f} \;=\; {}^{b}\boldsymbol{a} + {}^{b}_{n}\boldsymbol{R}\,{}^{n}\boldsymbol{g}. $$

The vector ${}^{b}\boldsymbol{y} \in \mathbb{R}^6$ is the signal of interest corrupted by a slowly changing bias ${}^{b}\boldsymbol{b}^{\top} = \begin{bmatrix} {}^{b}\boldsymbol{b}_a{}^{\top} & {}^{b}\boldsymbol{b}_g{}^{\top} \end{bmatrix}$ and measurement noise $\boldsymbol{n}$. The symbol ${}^{b}\boldsymbol{a}$ denotes the body frame acceleration of the rover. The symbol ${}^{n}\boldsymbol{g}$ is the gravity vector in the navigation frame, ${}^{n}\boldsymbol{g}^{\top} = \begin{bmatrix} 0 & 0 & g_e \end{bmatrix}$, $g_e \approx -9.78$ m/s/s. Since the sensor biases are slowly changing, for short periods of time (e.g. $\sim$ 10s), they are essentially constant. Hence we assume the IMU bias to be modeled as

$$ {}^{b}\dot{\boldsymbol{b}} = \boldsymbol{0}. $$

To estimate the biases, for improved navigation performance, we append the bias states to the navigation state to define the augmented state vector as

$$ \boldsymbol{x}^{\top} = \begin{bmatrix} \bar{\mathbf{x}}^{\top} & {}^{b}\boldsymbol{b}^{\top} \end{bmatrix}. \tag{1} $$

B. Error state vector

The differential equations that describe the evolution of (1) are nonlinear (see eqns. 11.38-11.40 in [3]). All practical real-time systems estimate the error in (1). The error state dynamic system can be linearized and hence can be estimated (assuming certain assumptions holds) using fast algorithms like the Extended Kalman Filter. Denote the INS error state vector as $\delta\boldsymbol{x}^{\top} = \begin{bmatrix} {}^{n}\delta\boldsymbol{p}_b^{\top} & {}^{n}\delta\boldsymbol{v}_b^{\top} & {}^{n}\boldsymbol{\rho}^{\top} & {}^{b}\delta\boldsymbol{b}_g^{\top} & {}^{b}\delta\boldsymbol{b}_a^{\top} \end{bmatrix}$ consisting of errors in position, velocity, small angle rotation, gyroscope bias and accelerometer bias. The small angle rotation ${}^{n}\boldsymbol{\rho}$ denotes the transformation from the estimated rotation to the actual rotation from the body to the navigation frame, via $\boldsymbol{I} + [{}^{n}\boldsymbol{\rho}\times]$, given by

$$ {}^{n}_{b}\boldsymbol{R} = (\boldsymbol{I} + [{}^{n}\boldsymbol{\rho}\times])\,{}^{n}_{b}\hat{\boldsymbol{R}}. $$

The linearized error state differential equations are given by [3]

$$ \begin{aligned} {}^{n}\delta\dot{\boldsymbol{p}}_b &= {}^{n}\delta\boldsymbol{v}_b && (2)\\ {}^{n}\delta\dot{\boldsymbol{v}}_b &= -[{}^{n}\boldsymbol{f}\times]\,{}^{n}\boldsymbol{\rho} + {}^{n}_{b}\boldsymbol{R}\,{}^{b}\delta\boldsymbol{b}_a && (3)\\ {}^{n}\dot{\boldsymbol{\rho}} &= {}^{n}_{b}\boldsymbol{R}\,{}^{b}\delta\boldsymbol{b}_g && (4)\\ {}^{b}\delta\dot{\boldsymbol{b}}_a &= \boldsymbol{0} && (5)\\ {}^{b}\delta\dot{\boldsymbol{b}}_g &= \boldsymbol{0} && (6) \end{aligned} $$

where the additive noises have been ignored since they are irrelevant to observability analysis.

C. State transition matrix

The set of differential equations given by $(2-6)$ can be solved in closed form. Let $t_0 \geq 0$ be the initial time. The differential equations in $(2-6)$ can be written as a linear function of $\delta\boldsymbol{x}$ for all $t > t_0$ as

$$ \delta\dot{\boldsymbol{x}}(t) = \boldsymbol{A}(t)\delta\boldsymbol{x}(t) \tag{7} $$

where

$$ \boldsymbol{A}(t) = \begin{bmatrix} \boldsymbol{0} & \boldsymbol{I} & \boldsymbol{0} & \boldsymbol{0} & \boldsymbol{0} \\ \boldsymbol{0} & \boldsymbol{0} & -[{}^{n}\boldsymbol{f}\times] & \boldsymbol{0} & {}^{n}_{b}\boldsymbol{R} \\ \boldsymbol{0} & \boldsymbol{0} & \boldsymbol{0} & {}^{n}_{b}\boldsymbol{R} & \boldsymbol{0} \\ \boldsymbol{0} & \boldsymbol{0} & \boldsymbol{0} & \boldsymbol{0} & \boldsymbol{0} \\ \boldsymbol{0} & \boldsymbol{0} & \boldsymbol{0} & \boldsymbol{0} & \boldsymbol{0} \end{bmatrix}. \tag{8} $$

Let $\boldsymbol{\Phi}(t, t_0)$ be the state transition matrix corresponding to the dynamic model in (7). The state transition matrix satisfies

$$ \dot{\boldsymbol{\Phi}}(t, t_0) = \boldsymbol{A}(t)\boldsymbol{\Phi}(t, t_0) \tag{9} $$

for all $t > t_0$. Since $\boldsymbol{A}$ is an upper triangular matrix, it is possible to solve (9) in closed form as

$$ \boldsymbol{\Phi}(t, t_0) = \begin{bmatrix} \boldsymbol{I} & (t-t_0)\boldsymbol{I} & \boldsymbol{\mathcal{P}}_t & \boldsymbol{\mathcal{T}}_t & \boldsymbol{\mathcal{Q}}_t \\ \boldsymbol{0} & \boldsymbol{I} & -\boldsymbol{\mathcal{S}}_t & \boldsymbol{\mathcal{M}}_t & \boldsymbol{\mathcal{R}}_t \\ \boldsymbol{0} & \boldsymbol{0} & \boldsymbol{I} & \boldsymbol{\mathcal{R}}_t & \boldsymbol{0} \\ \boldsymbol{0} & \boldsymbol{0} & \boldsymbol{0} & \boldsymbol{I} & \boldsymbol{0} \\ \boldsymbol{0} & \boldsymbol{0} & \boldsymbol{0} & \boldsymbol{0} & \boldsymbol{I} \end{bmatrix} \tag{10} $$

where

$$ \begin{aligned} \boldsymbol{\mathcal{R}}_t &= \int_{t_0}^{t} {}^{n}_{b(\tau)}\boldsymbol{R}\,d\tau & \boldsymbol{\mathcal{S}}_t &= \int_{t_0}^{t} [{}^{n}\boldsymbol{f}(\tau)\times]\,d\tau \\ \boldsymbol{\mathcal{P}}_t &= -\int_{t_0}^{t} \boldsymbol{\mathcal{S}}_s\,ds & \boldsymbol{\mathcal{Q}}_t &= \int_{t_0}^{t} \boldsymbol{\mathcal{R}}_s\,ds \\ \boldsymbol{\mathcal{M}}_t &= -\int_{t_0}^{t} [{}^{n}\boldsymbol{f}(s)\times]\,\boldsymbol{\mathcal{R}}_s\,ds & \boldsymbol{\mathcal{T}}_t &= \int_{t_0}^{t} \boldsymbol{\mathcal{M}}_r\,dr \end{aligned} $$

D. Measurement model

When the vehicle is detected to be stationary, we create the following pseudo-measurements:

1) Zero velocity update: The measurement is ${}^{n}\tilde{\boldsymbol{v}}_b = \boldsymbol{0}$. The measurement residual is computed as ${}^{n}\delta\boldsymbol{v}_b = -{}^{n}\hat{\boldsymbol{v}}_b$ and modeled as

$$ {}^{n}\delta\boldsymbol{v}_b = \boldsymbol{H}_v\delta\boldsymbol{x} $$

where $\boldsymbol{H}_v = \begin{bmatrix} \boldsymbol{0} & \boldsymbol{I} & \boldsymbol{0} & \boldsymbol{0} & \boldsymbol{0} \end{bmatrix}$.

2) Zero angular rate update: The measurement is ${}^{b}\tilde{\boldsymbol{\omega}}_{nb} = \boldsymbol{0}$. The measurement residual is derived as

$$ \begin{aligned} {}^{b}\delta\boldsymbol{\omega}_{nb} &= {}^{b}\boldsymbol{\omega}_{nb} - {}^{b}\hat{\boldsymbol{\omega}}_{nb} \\ &= {}^{b}\boldsymbol{\omega}_{ib} - {}^{b}\boldsymbol{\omega}_{in} - {}^{b}\hat{\boldsymbol{\omega}}_{ib} + {}^{b}\hat{\boldsymbol{\omega}}_{in} \\ &= {}^{b}\delta\boldsymbol{\omega}_{ib} - {}^{b}\delta\boldsymbol{\omega}_{in} \end{aligned} \tag{11} $$

where ${}^{b}\delta\boldsymbol{\omega}_{in} = [{}^{b}_{e}\hat{\boldsymbol{R}}\,{}^{e}\boldsymbol{\omega}_{ie}\times]{}^{b}_{n}\hat{\boldsymbol{R}}\,{}^{n}\boldsymbol{\rho}$ and

$$ {}^{b}\delta\boldsymbol{\omega}_{ib} \;=\; -{}^{b}\delta\boldsymbol{b}_g \tag{12} $$

The term ${}^{b}\delta\boldsymbol{\omega}_{in}$ is ignored because ${}^{e}\boldsymbol{\omega}_{ie}{}^{\top} = \begin{bmatrix} 0 & 0 & 7.29\times10^{-5} \end{bmatrix}$ rad/s is smaller than the gyroscope measurement noise power spectral density for Micro-Electro-Mechanical Systems (MEMS) based instruments (for e.g. 180 deg/hr/Hz$^{\frac{1}{2}}$). Substituting (12) into (11) we derive

$$ {}^{b}\delta\boldsymbol{\omega}_{nb} = \boldsymbol{H}_{\omega}\delta\boldsymbol{x} $$

where $\boldsymbol{H}_{\omega} = \begin{bmatrix} \boldsymbol{0} & \boldsymbol{0} & \boldsymbol{0} & -\boldsymbol{I} & \boldsymbol{0} \end{bmatrix}$.

III. Observability analysis

The state at time t_0, denoted by $\delta\boldsymbol{x}(t_0)$ is observable from measurements $\delta y(t) = \boldsymbol{H}\delta\boldsymbol{x}(t)$ for time $t \geq t_0$, if and only if the observability gramian, given by

$$\boldsymbol{\mathcal{O}} = \int_{t_0}^{t} \boldsymbol{\Phi}(t,\tau)^\top \boldsymbol{H}^\top \boldsymbol{H}\boldsymbol{\Phi}(t,\tau)d\tau \tag{13}$$

is non-singular [10]. Further (13) is non-singular if and only if

$$\boldsymbol{H}\boldsymbol{\Phi}(t,\tau)\boldsymbol{x}(\tau) = \boldsymbol{0} \Rightarrow \boldsymbol{x}(\tau) = \boldsymbol{0}. \tag{14}$$

for all $\tau \in [t_0, t]$

Proposition 3.1: A vector $\boldsymbol{x} \in null\,(\boldsymbol{H}\boldsymbol{\Phi}(t,\tau))$ for all $\tau \in (t_0, t)$ if and only if $\boldsymbol{x} \in null\,(\boldsymbol{\mathcal{O}})$.

Proof: ($\Rightarrow$) Assume that there exists a vector $\boldsymbol{x}$ such that for all $\tau \in (t_0, t)$, $\boldsymbol{x} \in null\,(\boldsymbol{H}\boldsymbol{\Phi}(t,\tau))$. Then

$$\boldsymbol{\mathcal{O}}\boldsymbol{x} = \int_{t_0}^{t} \boldsymbol{\Phi}(t,\tau)^\top \boldsymbol{H}^\top \boldsymbol{H}\boldsymbol{\Phi}(t,\tau)\boldsymbol{x}d\tau = \boldsymbol{0}$$

Hence $\boldsymbol{x} \in null(\boldsymbol{\mathcal{O}})$.

($\Leftarrow$) On the other hand, if $\boldsymbol{x} \in null(\boldsymbol{\mathcal{O}})$, then $\boldsymbol{x}^\top\boldsymbol{\mathcal{O}}\boldsymbol{x} = 0$. We can rewrite $\boldsymbol{x}^\top\boldsymbol{\mathcal{O}}\boldsymbol{x}$ as

$$\begin{aligned} \boldsymbol{x}^\top\boldsymbol{\mathcal{O}}\boldsymbol{x} &= \int_{t_0}^{t} \boldsymbol{x}^\top\boldsymbol{\Phi}(t,\tau)^\top \boldsymbol{H}^\top \boldsymbol{H}\boldsymbol{\Phi}(t,\tau)\boldsymbol{x}d\tau \\ &= \int_{t_0}^{t} ||\boldsymbol{H}\boldsymbol{\Phi}(t,\tau)\boldsymbol{x}||^2 d\tau \\ &= 0. \end{aligned} \tag{15}$$

From (15) we conclude $\boldsymbol{H}\boldsymbol{\Phi}(t,\tau)\boldsymbol{x} = \boldsymbol{0}$ for all $\tau \in D$, where D is dense subset of (t_0, t). But since $\boldsymbol{H}\boldsymbol{\Phi}\boldsymbol{x}$ is continuous in t its behavior on (t_0, t) is fully described by its behavior on D. Therefore $\boldsymbol{H}\boldsymbol{\Phi}(t,\tau)\boldsymbol{x} = \boldsymbol{0}$ for all $\tau \in (t_0, t)$. Thus $\boldsymbol{x} \in null(\boldsymbol{H}\boldsymbol{\Phi}(t,\tau))$ for all $\tau \in (t_0, t)$. ■

In the next subsection we describe various motion scenarios under which observability conditions are analyzed.

A. Motion scenarios

Without loss of generality, we assume $t_0 = 0$ in all subsequent analysis. We define the total time of interest as $U = [0, t]$ over which the inertial measurements ${}^b\boldsymbol{f}$ and ${}^b\boldsymbol{\omega}_{ib}$ are defined. Let $M \subseteq U$ be the times when the rover is in motion and $S = U \setminus M$ be the times when the rover is stationary. Assume that the rover is equipped with stationary updates for all $\tau \in S$. If the rover is a land vehicle then as long as there is no wheel slip, it can accelerate only along the vehicle forward axis, denoted by ${}^b\boldsymbol{d}^\top = \begin{bmatrix} 1 & 0 & 0 \end{bmatrix}$.

The following motion scenarios are defined:

1) Stationary rover: In this case the rover is stationary for all $t \in U$, hence $S = U$ and $M = \emptyset$. The specific force in the navigation frame is given by
$${}^n\boldsymbol{f} = {}^n\boldsymbol{g}$$
and the rotation ${}^n_b\boldsymbol{R}$ is time invariant for all $\tau \in U$.
2) Rover decelerating to a stop: Let the rover be in motion in $M = [0, t_1)$, where $t_1 > 0$ is known. Hence $S = U \setminus M = [t_1, t]$. The specific force in the navigation frame is given by
$${}^n\boldsymbol{f} = \begin{cases} \kappa(\tau)\ {}^n_b\boldsymbol{R}\ {}^b\boldsymbol{d} + {}^n\boldsymbol{g} & \tau \in M \\ {}^n\boldsymbol{g} & \tau \in S \end{cases} \tag{16}$$
where κ is a smooth real valued function whose support lies in M. The rotation ${}^n_b\boldsymbol{R}$ is time invariant in S and possibly time varying in M.
3) Rover starting and ending in stationarity: Let t_1, t_2 satisfy $0 < t_1 < t_2 < t$. Assume that the rover was stationary in $S_1 = [0, t_1]$, $S_2 = [t_2, t]$ and in motion in $M = U \setminus (S_1 \cup S_2)$. The specific force in the navigation frame is given by
$${}^n\boldsymbol{f} = \begin{cases} \kappa(\tau)\ {}^n_b\boldsymbol{R}\ {}^b\boldsymbol{d} + {}^n\boldsymbol{g} & \tau \in M \\ {}^n\boldsymbol{g} & \tau \in S_1 \cup S_2 \end{cases}. \tag{17}$$
We can further divide this scenario into two sub-cases based on rotation in M as follows:
   a) If there is no rotation for all $\tau \in M$ then ${}^n_b\boldsymbol{R}$ is time invariant for all $\tau \in U$.
   b) If the rover undergoes rotation in M then ${}^n_b\boldsymbol{R}$ is time varying and its behavior is governed by
   $${}^n_b\dot{\boldsymbol{R}} = {}^n_b\boldsymbol{R}\left[{}^b\boldsymbol{\omega}_{nb}\times\right].$$
   Usually the vehicle can have significant rotation only along one axis (i.e. yaw rate), hence ${}^b\boldsymbol{\omega}_{nb}$ is along a single direction.

In Section III-B, we derive the right null space of $\boldsymbol{H}\boldsymbol{\Phi}(t,\tau)$ under various motion and aiding scenarios. Once the null space of $\boldsymbol{H}\boldsymbol{\Phi}(t,\tau)$ is determined, we can use Proposition 3.1 to conclude the same for $\boldsymbol{\mathcal{O}}$.

B. Observability using Stationary updates

In this subsection we derive the observability conditions for the INS error states using stationary updates. Errors in positions are not observable using stationary updates and hence the unobservable subspace is at least 3 dimensional. For this reason, we remove position error states from the original error state vector $\delta\boldsymbol{x}$. In all subsequent analysis in this subsection, the reduced state vector, state transformation and measurement projection matrix are given by

$$\begin{aligned} \delta\boldsymbol{x}_m^\top &= \begin{bmatrix} {}^n\delta\boldsymbol{v}_b^\top & {}^n\boldsymbol{\rho}^\top & {}^b\delta\boldsymbol{b}_g^\top & {}^b\delta\boldsymbol{b}_a^\top \end{bmatrix} \\ \boldsymbol{\Phi}_m(t,\tau) &= \begin{bmatrix} \boldsymbol{I} & -\boldsymbol{\mathcal{S}}_\tau & \boldsymbol{\mathcal{M}}_\tau & \boldsymbol{\mathcal{R}}_\tau \\ \boldsymbol{0} & \boldsymbol{I} & \boldsymbol{\mathcal{R}}_\tau & \boldsymbol{0} \\ \boldsymbol{0} & \boldsymbol{0} & \boldsymbol{I} & \boldsymbol{0} \\ \boldsymbol{0} & \boldsymbol{0} & \boldsymbol{0} & \boldsymbol{I} \end{bmatrix} \end{aligned} \tag{18}$$

$$\boldsymbol{H}_m = \begin{bmatrix} \boldsymbol{I} & \boldsymbol{0} & \boldsymbol{0} & \boldsymbol{0} \\ \boldsymbol{0} & \boldsymbol{0} & -\boldsymbol{I} & \boldsymbol{0} \end{bmatrix} \tag{19}$$

where $\tau \in U$. Observability of error states is discussed for the motion scenarios outlined in Section III-A:

1) Stationary rover: This scenario is a standard case often discussed in literature [3], [6], [8], [9] etc.

Proposition 3.2: If stationary updates are available for all $\tau \in S = U$, then there exists a 3 dimensional unobservable subspace spanned by

$$\left[\begin{array}{cccc} \mathbf{0}^\top & \boldsymbol{e}_i^\top & \mathbf{0}^\top & -\boldsymbol{e}_i^\top [{}^n\boldsymbol{g}\times]{}^n_b\boldsymbol{R} \end{array}\right]^\top \tag{20}$$

where $\boldsymbol{e}_i$ for $1 \leq i \leq 3$ is a basis for $\mathbb{R}^3$.

Proof: Under the conditions of the proposition the modified state transition, $\boldsymbol{\Phi}_m(\tau, 0)$ in (10) can be simplified as

$$\boldsymbol{\Phi}_m(\tau,0) = \left[\begin{array}{cccc} \boldsymbol{I} & -\tau[{}^n\boldsymbol{g}\times] & -\frac{\tau^2}{2}[{}^n\boldsymbol{g}\times]{}^n_b\boldsymbol{R} & \tau\,{}^n_b\boldsymbol{R} \\ \mathbf{0} & \boldsymbol{I} & {}^n_b\boldsymbol{R}\tau & \mathbf{0} \\ \mathbf{0} & \mathbf{0} & \boldsymbol{I} & \mathbf{0} \\ \mathbf{0} & \mathbf{0} & \mathbf{0} & \boldsymbol{I} \end{array}\right]. \tag{21}$$

Using (19) and (21) we derive

$$\boldsymbol{H}_m\boldsymbol{\Phi}_m(\tau,0) = \left[\begin{array}{cccc} \boldsymbol{I} & -[{}^n\boldsymbol{g}\times]\tau & -\frac{1}{2}[{}^n\boldsymbol{g}\times]{}^n_b\boldsymbol{R}\tau^2 & {}^n_b\boldsymbol{R}\tau \\ \mathbf{0} & \mathbf{0} & -\boldsymbol{I} & \mathbf{0} \end{array}\right]. \tag{22}$$

Let $\boldsymbol{v}_1^\top = \left[\begin{array}{cccc} \boldsymbol{u}_{11}^\top & \boldsymbol{u}_{12}^\top & \boldsymbol{u}_{13}^\top & \boldsymbol{u}_{14}^\top \end{array}\right]$ be an element of the right null space of (22) for all $\tau \in S$. Using $\boldsymbol{H}_m\boldsymbol{\Phi}_m\boldsymbol{v}_1 = \mathbf{0}$ we derive

$$\boldsymbol{u}_{13} = \mathbf{0} \tag{23}$$

$$\boldsymbol{u}_{11} - \tau[{}^n\boldsymbol{g}\times]\boldsymbol{u}_{12} + \tau\,{}^n_b\boldsymbol{R}\boldsymbol{u}_{14} = \mathbf{0}. \tag{24}$$

Substituting $\tau = 0$ into (24) we derive

$$\boldsymbol{u}_{11} = \mathbf{0}. \tag{25}$$

Differentiating (24), we derive

$$\boldsymbol{u}_{14} = {}^b_n\boldsymbol{R}[{}^n\boldsymbol{g}\times]\boldsymbol{u}_{12} \tag{26}$$

for all $\tau \in (0, t)$. Using (23), (25) and (26) we derive a basis of unobservable subspace as (20). ■

It is known that, when the rover is stationary with GPS position updates for all $\tau \in S$, we have a 4 dimensional unobservable subspace spanned by

$$\left[\begin{array}{cccc} \mathbf{0}^\top & \mathbf{0}^\top & {}^b\boldsymbol{g}^\top & \mathbf{0}^\top \\ \mathbf{0}^\top & \boldsymbol{e}_i^\top & \mathbf{0}^\top & -\boldsymbol{e}_i^\top[{}^n\boldsymbol{g}\times]{}^n_b\boldsymbol{R} \end{array}\right]^\top. \tag{27}$$

Using Proposition 3.2, we see that with the addition of stationary updates, errors in the 4 dimensional subspace spanned by (27) are driven to a 3 dimensional unobservable subspace spanned by (20).

2) Rover decelerating to a stop: The following proposition is proved:

Proposition 3.3: Let the motion conditions be as described in Item 2, Section III-A. If the rover is equipped with stationary updates for all $\tau \in S$, there exists a 3 dimensional unobservable subspace spanned by

$$\left[\begin{array}{cccc} \boldsymbol{e}_i^\top\boldsymbol{m}^\top(t_1) & \boldsymbol{e}_i^\top & \mathbf{0}^\top & -\boldsymbol{e}_i^\top[{}^n\boldsymbol{g}\times]{}^n_{b(t_1)}\boldsymbol{R} \end{array}\right] \tag{28}$$

where

$$\boldsymbol{m}(t_1) = \int_0^{t_1} \left\{\kappa\,[{}^n_b\boldsymbol{R}\,{}^b\boldsymbol{d}\times] + [{}^n\boldsymbol{g}\times] - {}^n_b\boldsymbol{R}\,{}^{b(t_1)}_n\boldsymbol{R}[{}^n\boldsymbol{g}\times]\right\} ds. \tag{29}$$

Proof: Let $\boldsymbol{v}_2^\top = \left[\begin{array}{cccc} \boldsymbol{u}_{21}^\top & \boldsymbol{u}_{22}^\top & \boldsymbol{u}_{23}^\top & \boldsymbol{u}_{24}^\top \end{array}\right]$ be an element of the right null space of $\boldsymbol{H}_{\boldsymbol{m}}\boldsymbol{\Phi}_{\boldsymbol{m}}(\tau, 0)$ in S. Equating $\boldsymbol{H}_{\boldsymbol{m}}\boldsymbol{\Phi}_{\boldsymbol{m}}\boldsymbol{v}_{\boldsymbol{2}}(\tau, 0) = \mathbf{0}$ we derive

$$\boldsymbol{u}_{23} = \mathbf{0} \tag{30}$$

$$\boldsymbol{u}_{21} - \int_0^\tau [{}^n\boldsymbol{f}\times]\boldsymbol{u}_{22}ds + \int_0^\tau {}^n_b\boldsymbol{R}\boldsymbol{u}_{24}ds = \mathbf{0} \tag{31}$$

for all $\tau \in S$. Differentiating (31) with respect to τ we derive

$$-[{}^n\boldsymbol{f}(\tau)\times]\boldsymbol{u}_{22} + {}^n_{b(\tau)}\boldsymbol{R}\boldsymbol{u}_{24} = \mathbf{0} \tag{32}$$

for all $\tau \in (t_1, t)$. We can rewrite (31) as

$$\boldsymbol{u}_{21} - \int_0^{t_1} [{}^n\boldsymbol{f}\times]\boldsymbol{u}_{22}ds + \int_0^{t_1} {}^n_b\boldsymbol{R}\boldsymbol{u}_{24}ds + \int_{t_1}^{\tau} \left(-[{}^n\boldsymbol{f}\times]\boldsymbol{u}_{22} + {}^n_b\boldsymbol{R}\boldsymbol{u}_{24}\right) ds = \mathbf{0}. \tag{33}$$

Noting that $\tau > t_1$ we substitute (32) into (33) to derive

$$\boldsymbol{u}_{21} - \int_0^{t_1} [{}^n\boldsymbol{f}\times]\boldsymbol{u}_{22}ds + \int_0^{t_1} {}^n_b\boldsymbol{R}\boldsymbol{u}_{24}ds = \mathbf{0}. \tag{34}$$

Since ${}^n\boldsymbol{f}(\tau) = {}^n\boldsymbol{g}$ and ${}^n_{b(\tau)}\boldsymbol{R} = {}^n_{b(t_1)}\boldsymbol{R}$ for all $\tau \in S$ we rewrite (32) as

$$\boldsymbol{u}_{24} = {}^{b(t_1)}_n\boldsymbol{R}[{}^n\boldsymbol{g}\times]\boldsymbol{u}_{22} \tag{35}$$

Substituting (35) and (16) into (34) we derive

$$\boldsymbol{u}_{21} = \boldsymbol{m}(t_1)\boldsymbol{u}_{22} \tag{36}$$

where $\boldsymbol{m}(t_1)$ is given by (29). From (30), (35) and (36) a basis for the unobservable subspace is computed as (28). ■

Note that Section III-B.1 is a special case of Section III-B.2. This is observed by setting $\kappa = 0$ (i.e. Stationary for all $\tau \in U$) in (16). The basis derived in (20) can also be derived by setting $\kappa = 0$ in (28).

3) Rover starting and ending stationary: Let $\boldsymbol{v}_3^\top = \left[\begin{array}{cccc} \boldsymbol{u}_{31}^\top & \boldsymbol{u}_{32}^\top & \boldsymbol{u}_{33}^\top & \boldsymbol{u}_{34}^\top \end{array}\right]$ be an element of the right null space of $\boldsymbol{H}_{\boldsymbol{m}}\boldsymbol{\Phi}_{\boldsymbol{m}}(\tau, 0)$ for all $\tau \in S_1 \cup S_2$. By Proposition 3.2, if we are equipped with stationary updates in S_1, then the unobservable subspace is given by (20), hence

$$\boldsymbol{u}_{31} = \mathbf{0} \tag{37}$$

$$\boldsymbol{u}_{33} = \mathbf{0} \tag{38}$$

$$\boldsymbol{u}_{34} = {}^{b(t_1)}_n\boldsymbol{R}[{}^n\boldsymbol{g}\times]\boldsymbol{u}_{32}. \tag{39}$$

For all $\tau \in S_2$ equating $\boldsymbol{H}_m\boldsymbol{\Phi}_m(\tau, 0)\boldsymbol{v}_3 = \mathbf{0}$ we derive

$$\int_0^\tau [{}^n\boldsymbol{f}\times]\boldsymbol{u}_{32} - {}^n_b\boldsymbol{R}\,\boldsymbol{u}_{34}ds = \mathbf{0}. \tag{40}$$

Differentiating (40) we derive

$$\boldsymbol{u}_{34} = {}^{b(t_2)}_{n}\boldsymbol{R}[{}^{n}\boldsymbol{g}\times]\boldsymbol{u}_{32} \tag{41}$$

for all $\tau \in (t_2, t)$. Substituting (39) and (41) into (40) we derive

$$\int_{t_1}^{t_2} [{}^{n}\boldsymbol{f}\times]\boldsymbol{u}_{32} - {}^{n}_{b}\boldsymbol{R}\ \boldsymbol{u}_{34} ds = \boldsymbol{0}. \tag{42}$$

Lemma 3.4: As ${}^{n}\boldsymbol{v}_b = \boldsymbol{0}$ for all $\tau \in S_1 \cup S_2$, $\int_{t_1}^{t_2} \kappa(\tau)\ {}^{n}_{b}\boldsymbol{R}\ {}^{b}\boldsymbol{d}\ d\tau = 0$.

Proof: By assumption we know that

$${}^{n}\boldsymbol{v}_b(t_2) = \boldsymbol{0}. \tag{43}$$

Further, for all $\tau \in U$ we derive

$${}^{n}\dot{\boldsymbol{v}}_b(\tau) = \kappa(\tau)\ {}^{n}_{b}\boldsymbol{R}^{b}\boldsymbol{d} \tag{44}$$

Using (44) we derive

$${}^{n}\boldsymbol{v}_b(t_2) = \int_{0}^{t_2} {}^{n}\dot{\boldsymbol{v}}_b d\tau = \int_{t_1}^{t_2} \kappa(\tau)\ {}^{n}_{b}\boldsymbol{R}\ {}^{b}\boldsymbol{d}\ d\tau. \tag{45}$$

The change in limits is because ${}^{n}\dot{\boldsymbol{v}}_b = \boldsymbol{0}$ for all $\tau \in S_1$. Using (43) and (45), the desired result is derived. ■

Re-writing (42) we derive

$$\int_{t_1}^{t_2} -[\boldsymbol{u}_{32}\times]\left(\kappa(\tau)\ {}^{n}_{b}\boldsymbol{R}\ {}^{b}\boldsymbol{d} + {}^{n}\boldsymbol{g}\right) - {}^{n}_{b}\boldsymbol{R}\ \boldsymbol{u}_{34} ds = \boldsymbol{0}. \tag{46}$$

Using Lemma 3.4 and (46) we derive

$$\int_{t_1}^{t_2} [{}^{n}\boldsymbol{g}\times]\boldsymbol{u}_{32} - {}^{n}_{b}\boldsymbol{R}\ \boldsymbol{u}_{34} ds = \boldsymbol{0}. \tag{47}$$

The following proposition derives a basis for unobservable subspace for item 3*a*, Section III-A:

Proposition 3.5: If ${}^{b}\boldsymbol{\omega}_{nb}(\tau) = \boldsymbol{0}$ for all $\tau \in M$, then there exists a 3 dimensional unobservable subspace spanned by

$$\begin{bmatrix} \boldsymbol{0}^\top & \boldsymbol{e}_i^\top & \boldsymbol{0}^\top & -\boldsymbol{e}_i^\top[{}^{n}\boldsymbol{g}\times]{}^{n}_{b}\boldsymbol{R} \end{bmatrix}^\top \tag{48}$$

where $\boldsymbol{e}_i$ for $1 \le i \le 3$ is a basis for $\mathbb{R}^3$.

Proof: Using (47) we derive

$$(t_2 - t_1)[{}^{n}\boldsymbol{g}\times]\boldsymbol{u}_{32} - (t_2 - t_1)\,{}^{n}_{b}\boldsymbol{R}\boldsymbol{u}_{34} = \boldsymbol{0} \tag{49}$$

Since $t_2 - t_1 > 0$, eqns. (49), (37) and (38) gives us the required basis for the unobservable subspace. ■

The following proposition derives a basis for unobservable subspace for item 3*b*, Section III-A:

Proposition 3.6: If the rover undergoes rotation along a single axis, ${}^{b}\boldsymbol{\omega}$, for $\tau \in M$, then the unobservable subspace is 1 dimensional spanned by

$$\begin{bmatrix} \boldsymbol{0}^\top & {}^{n}\boldsymbol{g}^\top & \boldsymbol{0}^\top & \boldsymbol{0}^\top \end{bmatrix}^\top \tag{50}$$

Proof: From (39) and (41) we derive

$$\boldsymbol{u}_{34} = {}^{b(t_2)}_{b(t_1)}\boldsymbol{R}\boldsymbol{u}_{34} \tag{51}$$

Since we have rotation only along ${}^{b}\boldsymbol{\omega}$, we conclude

$$\boldsymbol{u}_{34} = p\ {}^{b}\boldsymbol{\omega} \tag{52}$$

where p is a constant. Note that, for all $\tau \in M$

$${}^{n}_{b(\tau)}\boldsymbol{R} = \int_{t_1}^{\tau} {}^{n}_{b}\dot{\boldsymbol{R}} ds = \int_{t_1}^{\tau} {}^{n}_{b}\boldsymbol{R}[{}^{b}\boldsymbol{\omega}\times] dr \tag{53}$$

Substituting (53) and (52) into (47) we derive

$$(t_2 - t_1)[{}^{n}\boldsymbol{g}\times]\boldsymbol{u}_{32} = p\int_{t_1}^{t_2}\int_{t_1}^{s} {}^{n}_{b}\boldsymbol{R}[{}^{b}\boldsymbol{\omega}\times]{}^{b}\boldsymbol{\omega} dr ds = \boldsymbol{0}. \tag{54}$$

Since $t_2 - t_1 > 0$, using (54) we conclude

$$\boldsymbol{u}_{32} = q\ {}^{n}\boldsymbol{g} \tag{55}$$

where q is a constant. Substituting (55) into (39) we derive

$$\boldsymbol{u}_{34} = \boldsymbol{0}. \tag{56}$$

From (37), (38), (55) and (56) we derive the unobservable subspace to be (50). ■

As a corollary to Proposition 3.6, if we have velocity measurements (e.g. from GPS) in an arbitrarily small open subset of M then the unobservable subspace is trivial as long as the pitch (θ) of the rover is not $\pm\frac{\pi}{2}$ for any $\tau \in M$. It can be proved as follows:

Corollary 3.7: In addition to the conditions in Proposition 3.6, if $\theta \neq \pm\frac{\pi}{2}$ for all $\tau \in M$ and velocity measurements are available in an arbitrary open neighborhood $U_g \subset M$, then the unobservable subspace is trivial.

Proof: For all $\tau \in U_g$, equating $\boldsymbol{H}_m\boldsymbol{\Phi}_m\boldsymbol{v}_3 = \boldsymbol{0}$ we derive

$$\int_{0}^{\tau} [{}^{n}\boldsymbol{f}\times]\boldsymbol{u}_{32} - {}^{n}_{b}\boldsymbol{R}\ \boldsymbol{u}_{34} ds = \boldsymbol{0}. \tag{57}$$

Substituting (56) and (55) into (57) we derive

$$q\int_{t_0}^{\tau} \kappa[{}^{n}\boldsymbol{d}\times]{}^{n}\boldsymbol{g} ds = \boldsymbol{0} \tag{58}$$

where the limits are changed as ${}^{n}\boldsymbol{f} = {}^{n}\boldsymbol{g}$ for all $\tau \in S_1$. Since $\kappa \neq 0$ in M and $\theta \neq \pm\frac{\pi}{2}$ (i.e.${}^{n}\boldsymbol{d}$ and ${}^{n}\boldsymbol{g}$ cannot be collinear), we conclude $q = 0$. Substituting $q = 0$ into (55), we see that the unobservable subspace is trivial. ■

IV. Numerical analysis

This section numerically evaluates the observability of error states from a state estimation viewpoint. Rewriting $(2-6)$ after including process noise terms as

$$\begin{aligned}
{}^{n}\delta\dot{\boldsymbol{v}}_b &= -\left[{}^{n}\hat{\boldsymbol{f}}\times\right]{}^{n}\boldsymbol{\rho} + {}^{n}_{b}\hat{\boldsymbol{R}}\ {}^{b}\delta\boldsymbol{b}_a + {}^{n}_{b}\hat{\boldsymbol{R}}\ \boldsymbol{n}_a && (59)\\
{}^{n}\dot{\boldsymbol{\rho}} &= {}^{n}_{b}\hat{\boldsymbol{R}}\ {}^{b}\delta\boldsymbol{b}_g + {}^{n}_{b}\hat{\boldsymbol{R}}\ \boldsymbol{n}_g && (60)\\
{}^{b}\delta\dot{\boldsymbol{b}}_a &= \boldsymbol{n}_{b_a} && (61)\\
{}^{b}\delta\dot{\boldsymbol{b}}_g &= \boldsymbol{n}_{b_g} && (62)
\end{aligned}$$

where for reasons stated earlier ${}^{n}\delta\dot{\boldsymbol{p}}_b$ has been ignored. Let $\boldsymbol{N}^\top = \begin{bmatrix} \boldsymbol{n}_a^\top & \boldsymbol{n}_a^\top & \boldsymbol{n}_{b_a}^\top & \boldsymbol{n}_{b_g}^\top \end{bmatrix}$ denote the process

noise vector where $\boldsymbol{n}_a$, $\boldsymbol{n}_g$ denote the accelerometer and gyroscope measurement noise and $\boldsymbol{n}_{b_a}$, $\boldsymbol{n}_{b_g}$ denote the bias random walk parameters. Let $Q = Cov(N)$ be assumed to be a block diagonal with $block\_diag(\boldsymbol{Q}) = \begin{bmatrix} \boldsymbol{I}\sigma_a^2 & \boldsymbol{I}\sigma_g^2 & \boldsymbol{I}\sigma_{b_a}^2 & \boldsymbol{I}\sigma_{b_g}^2 \end{bmatrix}$. Similarly the measurement residual equations are modeled as

$$\delta\boldsymbol{y} = \boldsymbol{H}\delta\boldsymbol{x} + \boldsymbol{n}$$

where $\delta\boldsymbol{y}^\top = \begin{bmatrix} {}^n\delta\boldsymbol{v}_b^\top & {}^n\delta\boldsymbol{\omega}_{nb}^\top \end{bmatrix}$, $\boldsymbol{H}^\top = \begin{bmatrix} \boldsymbol{H}_v^\top & \boldsymbol{H}_\omega^\top \end{bmatrix}$ and $\boldsymbol{n}^\top = \begin{bmatrix} \boldsymbol{n}_v^\top & \boldsymbol{n}_\omega^\top \end{bmatrix}$ denotes additive white Gaussian measurement noise. It is assumed that $\boldsymbol{n} \sim \mathcal{N}(\boldsymbol{0}, \boldsymbol{R})$ with $block\_diag(\boldsymbol{R}) = \begin{bmatrix} \boldsymbol{I}\sigma_v^2 & \boldsymbol{I}\sigma_\omega^2 \end{bmatrix}$. The variance of the zero velocity update is selected as $\sigma_v^2 = 10^{-4}(\text{m/s})^2$. The variance of the zero angular rate update is selected as $\sigma_\omega^2 = 1 \times 10^{-6}(\text{rad/s})^2$. In the numerical analysis that follows, we use the decrease in parts of the covariance matrix $\boldsymbol{P}$ to indicate which portions of the error state become observable.

For the purpose of simulation we set $U = [0, 30]$ s. For motion scenarios described in Section III-A, the set S is described in the following table:

Motion scenario	S, seconds	Legend
1	$S = U$	Blue
2	$S = [0, 15]$	Red
$3a$ (${}^b\boldsymbol{\omega}_{nb} = \boldsymbol{0}$)	$S_1 = [0, 10]$, $S_2 = [20, 30]$	Black
$3b$ (${}^b\boldsymbol{\omega}_{nb} \neq \boldsymbol{0}$)	$S_1 = [0, 10]$, $S_2 = [20, 30]$	Magenta

The inertial measurements were integrated in discrete time at 100Hz. We assume we have stationary updates ${}^n\tilde{\boldsymbol{v}}_b, {}^b\tilde{\boldsymbol{\omega}}_{nb}$ at 1Hz for all discrete times $\tau_k \in S$. We implemented a discrete time fixed-point smoother to compute $E\{\boldsymbol{x}(0) | {}^n\tilde{\boldsymbol{v}}_b(\tau_k), {}^b\tilde{\boldsymbol{\omega}}_{nb}(\tau_k), \forall \tau_k \in S\}$ [5], [11]. The error standard deviation of the smoothed estimates is plotted as a time series in Figures 1-5. For all motion scenarios, the standard deviation of the smoothed estimates of the initial conditions is plotted only at times when measurement updates are available, for example in Figure 2, the magenta plot is absent during times $(10, 20)$ because there are no stationary updates in motion Scenario $3b$ at that time. It was assumed that the initial orientation of the rover is such that ${}^n_{b(0)}\hat{\boldsymbol{R}} = \boldsymbol{I}$. The initial uncertainty was selected as $block\_diag(Cov\{\delta\boldsymbol{x}\delta\boldsymbol{x}^\top\}) = \begin{bmatrix} \boldsymbol{I}\sigma_p^2 & \boldsymbol{I}\sigma_v^2 & \boldsymbol{I}\sigma_\rho^2 & \boldsymbol{I}\sigma_g^2 & \boldsymbol{I}\sigma_f^2 \end{bmatrix}$ where $\sigma_p = 1$m, $\sigma_v = 0.1$m/s, $\sigma_\rho = 10$deg, $\sigma_g = 10^{-5}$deg/s, and $\sigma_f = 10^{-3}$m/s/s.

Fig. 1 shows the uncertainty in the smoothed estimate of error in initial velocity. Since the observability conditions for errors in velocity in motion scenarios 1, $3a$ and $3b$ are the same, the blue, black and magenta plots overlap wherever defined. The red plot (Scenario 2) does not begin to decrease until $t = 15$, when stationary measurements become available. Even for $t > 15$, the standard deviation does not decrease to the same level as the other scenarios. This is because, even for $t > 15$, the initial velocity is not observable; instead, the error state vector has converged to an new unobservable subspace. The lack of observability in Scenario 2 is discussed in Proposition 3.3 which shows that the unobservable space includes a linear combination of

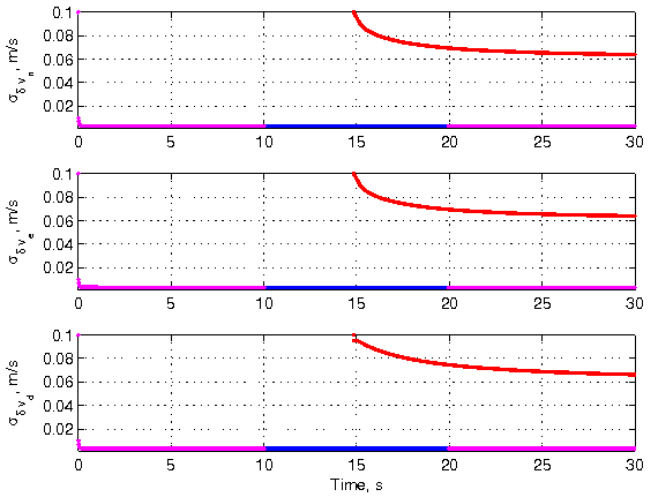

Fig. 1. Uncertainty in ${}^n\delta\hat{\boldsymbol{v}}_b^\top(0) = [\delta v_n \ \delta v_e \ \delta v_d]$ using all measurements in S.

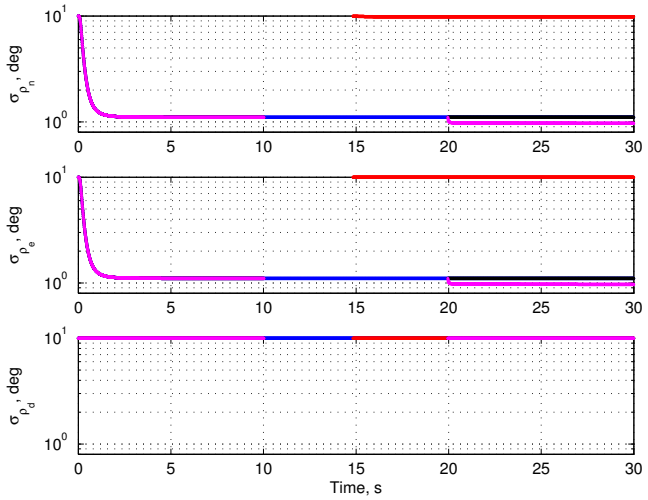

Fig. 2. Uncertainty in ${}^n\hat{\boldsymbol{\rho}}^\top(0) = [\rho_n \ \rho_e \ \rho_d]$ using all measurements in S.

velocity and yaw. The physical interpretation of this result, in this example, is that the knowledge that the vehicle is stationary for $t > 15$ and the inertial measurements for $t \in [0, 15]$ does not uniquely identify the initial velocity, because the yaw angle is unknown. Therefore, the direction of the initial velocity cannot be determined from the available data.

Fig. 2 shows the uncertainty in the smoothed estimate of ${}^n\boldsymbol{\rho}(0)$ using stationary measurements up to time t. In the interval $t \in [0, 10]$ s, there is no difference between Scenarios 1, $3a$ and $3b$. Hence the blue, black and magenta plots overlap in this time interval. Proposition 3.6 predicts that rotation along a single direction (yaw in this case) during M causes the first two components of the attitude error to

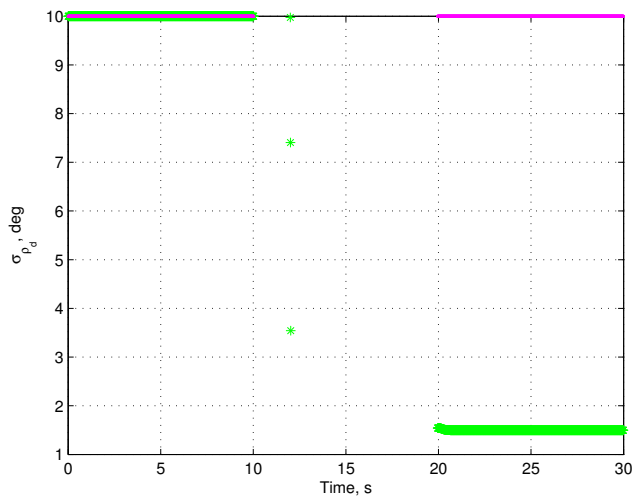

Fig. 3. Uncertainty in yaw direction after using stationary measurements in S is depicted by the solid magenta curve. In addition, if GNSS velocity measurements at introduced at three time instants in M, then the resultant uncertainty curve is shown by the green curve.

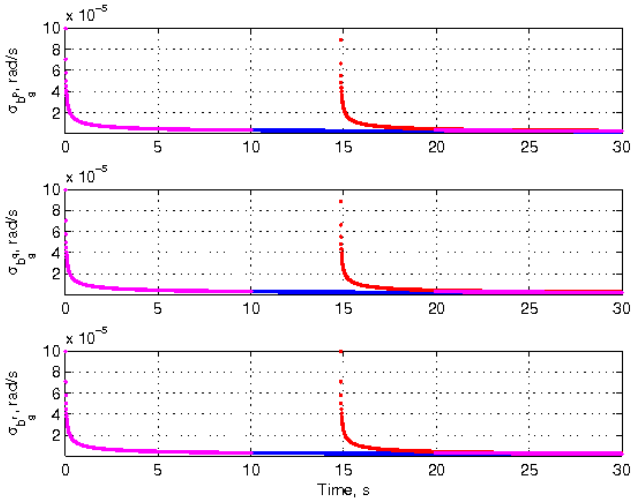

Fig. 4. Uncertainty in ${}^b\hat{\boldsymbol{b}}_g(0) = [b_g^p \;\; b_g^q \;\; b_g^r]$ using all measurements in S.

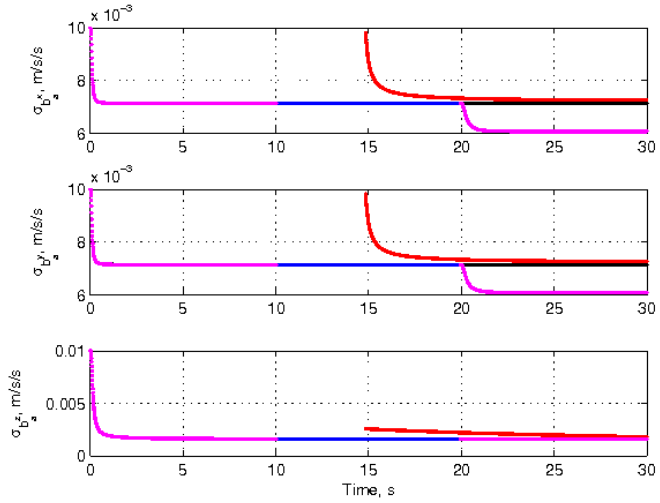

Fig. 5. Uncertainty in ${}^b\hat{\boldsymbol{b}}_a(0) = [b_a^x \;\; b_a^y \;\; b_a^z]$ using all measurements in S.

become observable. This is confirmed by the decrease in the first two components of the magenta plot compared to the black plot (Scenario 3a), after the rover enters stationary at time 20 s. Propositions 3.2, 3.3, 3.5 and 3.6 predict that initial errors in yaw direction are not observable. This is confirmed by the third subplot of Fig. 2, as the uncertainty in all scenarios stays constant.

On the other hand, Corollary 3.7 proves that the initial uncertainty in the yaw estimate is observable if velocity measurements are available during some $U_g \in M$. This is supported by Fig. 3. The magenta plot shows the uncertainty in motion Scenario 4, which is the same as the magenta plot in subplot 3 of Fig. 2. The green plot shows the uncertainty in the initial yaw estimate when velocity aiding is available at 3 time instants in M. The measurement standard deviation for the GPS velocity estimates is 2 cm/s.

Fig. 4 shows the uncertainty in the smoothed estimate in initial gyroscope bias. All motion scenarios have the same gyro bias observability characteristics and hence all plots converge to the same value.

Fig. 5 shows the uncertainty in the smoothed estimate of initial accelerometer bias. It is seen that the black and blue plots overlap since the observability characteristics in Scenario 1 and $3a$ are similar. Since the roll (ϕ), pitch (θ) and yaw (ψ) were all initialized to zero, i.e. $\phi = \theta = \psi = 0$, the error in the third component of accelerometer bias is always observable as the error is along ${}^n\boldsymbol{g}$ (ref. eqn. (20), (28), (48), (50)). It is interesting to note that, in motion Scenario $3b$ (magenta plot), the uncertainty in accelerometer bias in the first two directions decrease at time 20, when the rover enters stationary after undertaking a rotation. Hence the magenta plot confirms the results in Proposition 3.6 that errors in accelerometer biases are observable if we have rotation in one direction.

V. CONCLUSIONS

This paper analyzed the observability characteristics of stationary updates for typical maneuvers on a land vehicle (e.g. stationary rover, rover stopping at a traffic light, rover error state initialization by accelerating from rest and then stopping). The paper derived a basis for the unobservable subspace of the INS error state whenever applicable. The paper also shows simulation results that verify the theoretical conclusions in the paper. The results show the benefits of "stationary updates" when they can be reliably detected.

REFERENCES

[1] S. Y. Cho, B. D. Kim, Y. S. Cho, and W. S. Choi, "Observability analysis of the INS/GPS navigation system on the measurements in

land vehicle applications," in *Control, Automation and Systems, 2007. ICCAS '07. International Conference on*, October 2007, pp. 841–846.

[2] P. Davidson, J. Hautamki, J. Collin, and J. Takala, "Improved Vehicle Positioning in Urban Environment through Integration of GPS and Low-Cost Inertial Sensors."

[3] J. A. Farrell, *Aided Navigation: GPS with high rate sensors*. McGraw Hill, 2008.

[4] Foxlin, E., "Pedestrian tracking with shoe-mounted inertial sensors," *IEEE Computer Graphics and Applications*, vol. 25, no. 6, pp. 38–46, 2005.

[5] A. Gelb, *Applied Optimal Estimation*. Cambridge, Massachusetts: The M.I.T. Press, 1974.

[6] D. Goshen-Meskin and I. Bar-Itzhack, "Observability analysis of piece-wise constant systems with applications to inertial navigation," in *Proceedings of the 29th Conference on Decision and Control*, 1990, pp. 821–826.

[7] D. Grejner-Brzezinska, C. Toth, and Y. Yi, "Bridging GPS gaps in urban canyons: Can ZUPT really help?" in *Proceedings of the ION-GPS2001. Fairfax: The Institute of Navigation*, 2002.

[8] S. Hong, M. H. Lee, H.-H. Chun, S.-H. Kwon, and J. Speyer, "Observability of error States in GPS/INS integration," *Vehicular Technology, IEEE Transactions on*, vol. 54, no. 2, pp. 731–743, March 2005.

[9] S. Hong, M. H. Lee, J. Rios, and J. Speyer, "Observability analysis of GPS aided INS," *Proceeding of ION GPS, 2000*, pp. 2618 – 2624, September 2000.

[10] T. Kailath, *Linear Systems*. Prentice Hall Inc., 1980.

[11] J. S. Meditch, *Stochastic Optimal Linear Estimation and Control, First Edition*. McGraw-Hill Education, August 1969.

[12] O. Mezentsev, Y. Lu, G. Lachapelle, and R. Klukas, "Vehicular Navigation in Urban Canyons Using a High Sensitivity GPS Receiver Augmented with a Low Cost Rate Gyro," in *ION GPS*, 2002, pp. 24–26.

[13] L. Ojeda and J. Borenstein, "Non-GPS navigation with the personal dead-reckoning system," in *Proceedings of the SPIE Defense and Security Conference, Unmanned Systems Technology IX*, 2007.

[14] M. Petovello, O. Mezentsev, G. Lachapelle, and M. Cannon, "High sensitivity GPS velocity updates for personal indoor navigation using inertial navigation systems," *Proceedings of ION GPS/GNSS (September 9-12 2003, Portland OR)*, pp. 2886–2896, 2003.

[15] A. Ramanandan, A. Chen, J. Farrell, and S. S., "Detection of Stationarity in an Inertial Navigation System," *Proceedings of ION GPS/GNSS (September 21-24 2010, Portland OR)*, September 2010.

[16] I. Rhee, M. Abdel-Hafez, and J. Speyer, "Observability of an integrated GPS/INS during maneuvers," *Aerospace and Electronic Systems, IEEE Transactions on*, vol. 40, no. 2, pp. 526–535, April 2004.

[17] H. Yu, "An algorithm to detect zero-velocity in automobiles using accelerometer signals," Master of Science Thesis, Tampere University Of Technology, 2008.